Proximal-sensing-powered hydrological modelling of a vineyard: a scale analysis

N Paciolla[1], C Corbari[1], A Maltese[2], G Ciraolo[2], M Mancini[1]
[1]Politecnico, Milano – [2]Università di Palermo
nicola.paciolla@polimi.it

DEPARTMENT OF CIVIL AND ENVIRONMENTAL ENGINEERING

POLITECNICO MILANO 1863

1. Introduction

Day-to-day crop management requires extensive and comprehensive tools providing a full knowledge of the plants' status. Hydrological modelling allows to monitor the water mass exchanges in the soil-surface-atmosphere layer by characterizing the main driving forces that direct them. The EvapoTranspiration (ET), sum of the water freely evaporated from the soil and transpired through the plant leaf stomata, is often considered a handy proxy for plant irrigation demand. Recently, remote/proximal sensing (RPS) has improved hydrological modelling: data can be obtained with a relatively high temporal frequency (up to a daily basis) and with varying spatial resolutions (up to 10 m for satellite data, 100-1 cm for proximal sensing). Thus, the joint use of hydrological modelling and RPS can help define the management for irrigation water use optimization. The trade-off between data heterogeneity and data quality varies greatly: homogeneous crops (like maize) can be studied with field-size spatial resolution, while more heterogeneous crops (like arboreal cultivations) may require a distinction between the single plant and the surrounding terrain through higher-resolution data.

The main objective of this study is to determine the RPS-powered model sensitivity in terms of ET – hence of irrigation water requirements – with spatial resolution. The main investigation points are: (1) Is high resolution data strictly necessary to accurately model an area as heterogeneous as a vineyard? (2) Can a high-resolution calibration help the model to interpret low-resolution data?

2a. Case Study

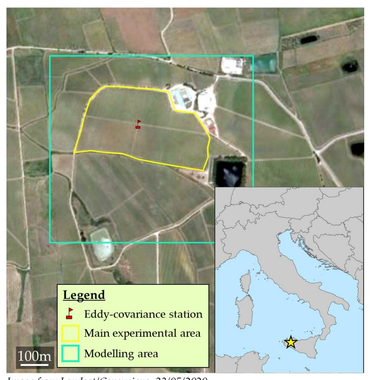

Image from Landsat/Copernicus, 23/05/2020

The study area is the experimental vineyard field of the Tenute Rapitalà farm in the territory of Camporeale (Sicily). Data refers to the Jun-Sep 2008 DIFA field campaign [1]. The yellow-bordered area identifies the main experimental field, hosting the eddy-covariance station. The vine rows are 2.4m apart and in each row the plants are positioned every 0.95m, resulting in a global plant density of 4386 plants per ha. The terrain shows a mild slope (<10%), SSW-oriented. The soil texture is classified as loam. Residual Water Content is 0.04 $m^3\ m^{-3}$, while Saturation Water Content is 0.45 $m^3\ m^{-3}$. Drop irrigation is the main irrigation practice for the area.

2b. Materials

Five airborne proximal sensing acquisitions have been carried out during the summer of 2008, with sampling height around 1000 m above ground level [1]. A multispectral camera has been used to retrieve the visible (VIS) and near-infrared (NIR) images, at 0.7 m spatial resolution; another, lower-resolution camera provided the thermal infrared (TIR) images at 1.7 m spatial resolution.

Simultaneous Leaf Area Index (LAI) and vegetation fraction (f_V) data have been gathered with an optoelectronics tool. Plant height information has been obtained from VIS data by means of an empirical relation calibrated in situ. Flight data is detailed in the Table on the right.

Plant growth is evident in the Vegetation Fraction, while variations on Albedo are less marked. Land Surface Temperature (LST) data highlights the cooler water basins against the cultivated fields and the warmer non-vegetated paths (as confirmed by the vegetation fraction low values). Some "patchwork" areas with strongly heterogeneous data can be detected in 22/07 and 22/08. As PS can be obtained by composition of different overpasses, some images can create conflicts due to slightly different atmospheric conditions at the acquisition times (e.g., some passing clouds). Finally, a flux tower was located at the centre of the experimental field [2]. It provided measurement of air temperature, humidity, precipitation and energy fluxes: Net Radiation (Rn), soil thermal flux (G), latent heat (L), sensible heat (H), available every 30 mins. The energy balance, although never closed, presents a good adaptation (slope=0.95, R^2=0.83).

Test days	11th Jun	3rd Jul	22nd Jul	22nd Aug	3rd Sep
DOYs (year 2008)	163	185	204	235	247
Meteorological data	●	●	●	*Partial*	●
Energy Fluxes	●	●	●	*Partial*	●
Flight time (local, UTC+2)	10:45	08:15	08:45	09:15	08:45
Land Surface Temperature	●	●	●	●	●
Calibration date	Yes	No	Yes	No	Yes
Validation date	Yes	Yes	No	Yes	Yes

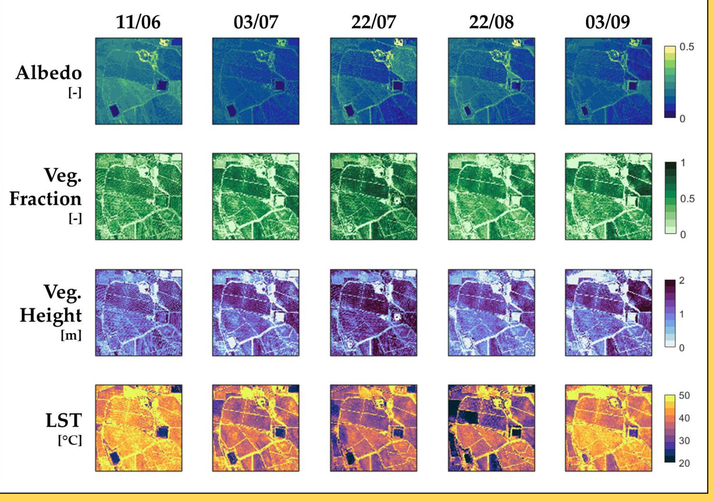

2c. Methods

The **FEST-EWB** distributed hydrological model [3] closes the water and energy balances pixel by pixel, computing the superficial runoff and routing the water through the hydrological network.

$$\begin{cases} \frac{\partial SM}{\partial t} = \frac{P - R - PE - ET}{dz}, & mass\ balance \\ Rn - G - (Hs + Hc) - (LEs + LEc) = \frac{\Delta W}{\Delta t}, & energy\ balance \end{cases}$$

The calibration of the model has been performed through the minimization of the average model error between modelled **Representative Equilibrium Temperature** (RET) and remotely-sensed **Land Surface Temperature** (LST). As the simulations are performed in summer days with no water input and in a restricted time span, the selected calibration parameters are the **minimum stomatal resistance** (rs_{MIN}) and the **soil surface resistance** (r_S), given their strong link to the energy partition mechanisms. The calibration/validation process is synchronous, since calibration (LST) and validation (energy fluxes) data are obtained from independent sources.

Eddy-covariance data are influenced by the aerodynamic conditions of the atmosphere bottom layer. Depending on the spatial resolution, measurement footprint computation may be required to aptly simulate the measurement performed by the instrument.

Scale analysis

1. Model outputs (L, H, SM and RET) are upscaled to some specific spatial resolutions.
2. Model input data is upscaled to the same resolution before running the FEST-EWB, which is calibrated anew for each run.
3. Model results, either originated from the upscaling of the native-resolution results (Upscaled Outputs, UO) or after the model calibration employing upscaled input data (Upscaled Inputs, UI), are compared

The scales have been chosen by similarity with some common satellite data: 10m for Sentinel, 30m for Landsat, 250m for MODIS VIS, 1km for MODIS TIR. To avoid reprojections, the actual analysis scales are multiples of 1.7m: 10.2m, 30.6m, 244.8m and 734.4m. The upscaling has been performed through successive averaging of the original data to the target resolutions.

4. Model calibration/validation

Model calibration

The calibration parameters have been corrected across numerous simulations with the aim of minimizing the temperature error. Originally, soil surface resistance was set to 500 s/m for all the pixels; minimum stomatal resistance, on the other hand, was set to 200 s/m (vineyard) for highly-vegetated pixels and to 50 s/m (grass) for the rest of the area, based on literature values.

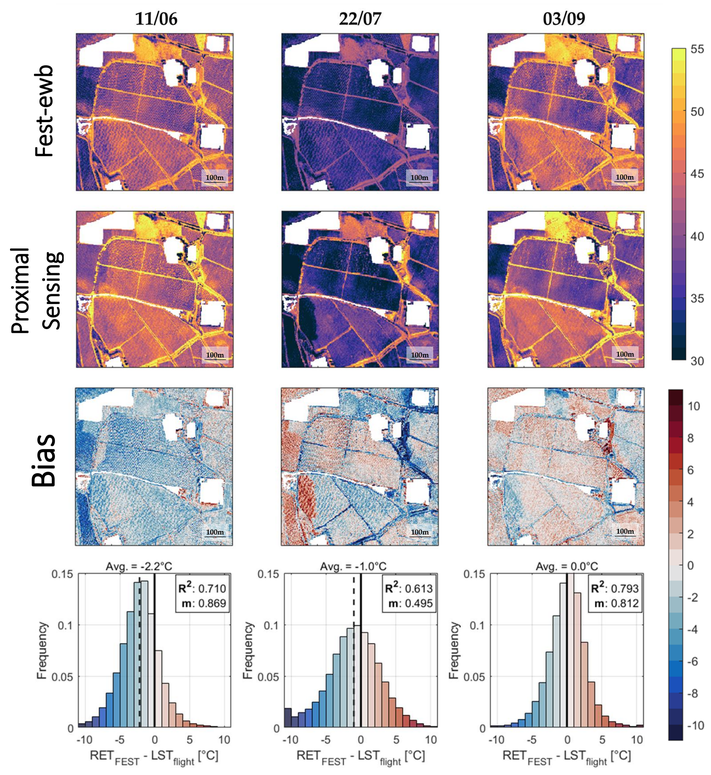

Parameter	Before Calibration		After Calibration	
Statistic	*Average*	*Min – Max*	*Average*	*Min – Max*
rs_{MIN}	128 s/m	50 – 200 s/m	606 s/m	50 – 1920 s/m
r_S	500 s/m	-	603 s/m	0 – 1920 s/m

RET-LST comparison results show a good correspondence, especially in the distinction between warmer bare-soil areas and cooler vegetated patches. Some areas have been blanked out, as not pertinent to the analysis (artificial basins, tarmac and buildings).

Model biases (difference between modelled RET and estimated LST) seem to be normally distributed around their average value, with most of the pixels (61%, 59% and 78% for each date, respectively) displaying an error within ±3°C of the target LST.

- 11th June seems to have a quite uniform error distribution,
- 22nd July shows important underestimation-errors in the non-vegetated areas,
- 3rd September displays a diffused overestimation in the vegetated part.

In all three dates, however, some "spot"-like errors are present, mostly found in the western part of the image. For these "spot"-like areas, the model error seems to be distinguished from that of the rest of the area: on 11th June, the model is much cooler than the LST in that area with respect to the central part of the test site, and on 22nd July a sudden change in model trend (from a sharp overestimation to a mild underestimation) is clearly visible. These problems may be due to the nature of the LST images employed, which can be conditioned by temporary cloud cover over the target area.

The adaptation statistics for the calibration process are detailed in the Table below. On the left-hand side, classic adaptation statistics are displayed: model-to-data bias, slope of the linear regression and determination coefficient (R^2). On the right-hand side, the surface temperature error (expressed in terms of Root Mean Square Error, RMSE) is sorted by vegetation density (in terms of Leaf Area Index, LAI) of the relative pixel. Generally, lower errors are found for medium-to-high vegetation levels, although the 11th June test date shows a less definite trend.

Date	Bias	Slope	R^2	RMSE [°C] sorted by LAI [m^2/m^2] (pixel num.)					Global RMSE
				< 0.5	*0.5 – 1*	*1 – 1.5*	*1.5 – 2*	*≥ 2*	
11th Jun	-2.2°C	0.869	.71	3.5 (18%)	2.8 (27%)	3.0 (22%)	3.8 (15%)	4.5 (17%)	3.5°C
22nd Jul	-1.0°C	0.495	.61	5.6 (13%)	4.4 (13%)	3.7 (16%)	3.4 (15%)	3.3 (42%)	3.9°C
3rd Sep	+0.0°C	0.812	.79	3.8 (25%)	2.7 (18%)	2.3 (20%)	2.0 (16%)	2.2 (22%)	2.8°C

Model validation

Among the FEST-EWB results, components of the energy balance for every pixel are available. A comparison with the quantities measured by the eddy-covariance instrument can be performed with the FEST-EWB outputs for the station own pixel and those extracted employing the eddy footprint. In the lower panels, Net Radiation (Rn) and Soil Heat Flux (G) are compared, with positive results. In the upper panels, for Latent Heat (L) and Sensible Heat (H), the footprint-filtered FEST-EWB outputs are shown. The presence of a consistent bare-soil area around the station is evident in the higher values of the Sensible Heat as opposed to the Latent Heat registered by the station. These dynamics are all well-captured by the model interpretation. The Table below details the Nash-Sutcliffe Efficiency scores for the flux validation.

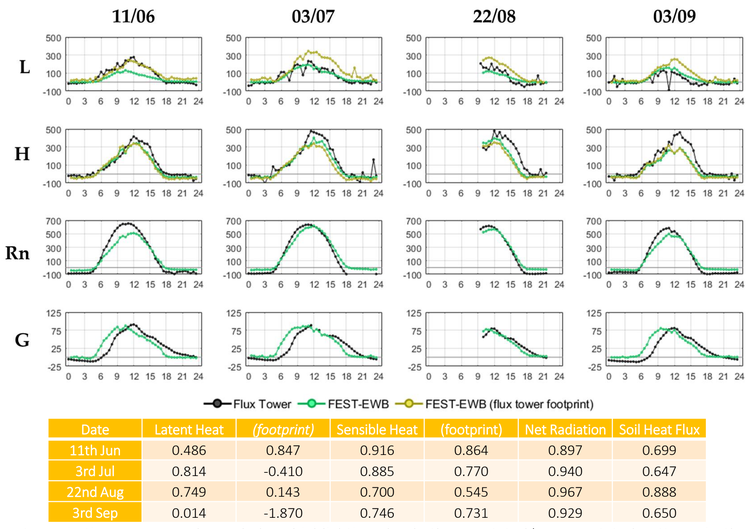

Date	Latent Heat	*(footprint)*	Sensible Heat	(footprint)	Net Radiation	Soil Heat Flux
11th Jun	0.486	0.847	0.916	0.864	0.897	0.699
3rd Jul	0.814	-0.410	0.885	0.770	0.940	0.647
22nd Aug	0.749	0.143	0.700	0.545	0.967	0.888
3rd Sep	0.014	-1.870	0.746	0.731	0.929	0.650

Daily evapotranspiration maps are shown below, highlighting clearly the vegetated/non-vegetated patterns in the main experimental area. Warmer days (July) show an overall higher ET output than early (June) or late (September) Summer. These outputs are critical for the definition of the field irrigation water requirement.

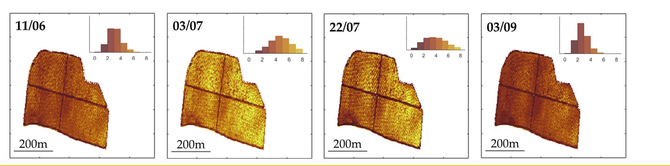

5a. Outputs & Inputs Upscaling

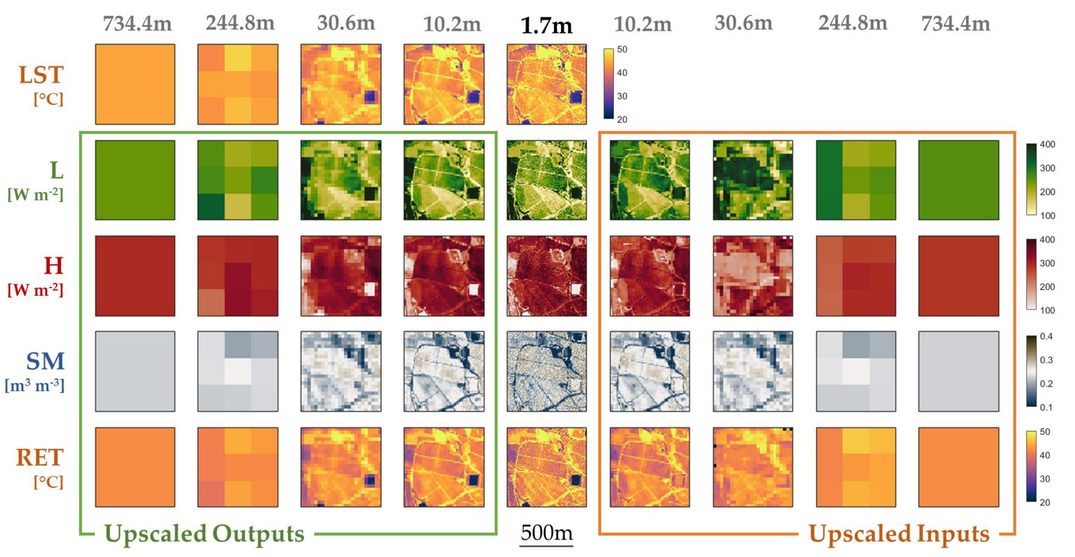

On the left, all the parameters involved in the scale analysis are presented, for the example 11th June date (11:00 local time): flight-sensed **Land Surface Temperature** (LST) and modelled **Latent Heat** (L), **Sensible Heat** (H), **Soil Moisture** (SM) and **Representative Equilibrium Temperature** (RET). Some surface heterogeneity features – like bare-soil paths – are preserved in the first step (10.2 m) and still distinguishable in the second (30.6 m), where the scale ratio is 18:1. From the third step (244.8 m) all heterogeneity is lost. Apart from absolute-value differences, both LST and RET are similarly affected by the upscaling process.

In the plot below, the effects of the upscaling processes are detailed. For each plot, the darkened area identifies the one-standard-deviation-range (±σ) around the average value. Being the 734.4 m step made up of just one pixel, all standard deviations are null at that stage.

In the Upscaling Outputs (UO) approach, as scales progress, the overall data average is unaffected, because of the intrinsic properties of the average operation. On the other hand, the standard deviation decreases with scale, as fewer pixels covering the same area determine a decreasing heterogeneity of the data.

- The positive model interpretation of the LST transpires from the similar shape of the RET and LST plots. The bias that separates them at the native resolution, detailed above, is preserved along the aggregation process.
- Latent Heat tends to be more widely distributed than Sensible Heat. This distinction holds until the 30.6 m threshold, with the two fluxes gaining similar heterogeneity by the 244.8 m step. This is consistent with the maps shown above, where the heterogeneity features are shown to hold until the 30.6 m upscaling step. The entity of these heterogeneity shifts is detailed in the Table below. For each product and each scale, the Variation Coefficient (standard deviation normalized over the average value) is shown, progressively decreasing with the increase of the spatial resolution.

In the Upscaling Inputs (UI) approach, data inputs have been upscaled to the different target scales before being employed in the model. Thus, after calibration, the model results are produced directly at the target scale, simulating the functioning of the model at coarser resolutions for the same data set. The effect of the calibration on the parameters is detailed in the Table below for all the calibration steps. The Variation Coefficient (an indirect measure of the dataset heterogeneity) stays high (above 50%) until the 30.6 m step, before plummeting to the 25% value of the 244.8 m scale. The calibration functions employed for the two parameters are practically the same, except for heavily-overestimated values. This distinction brings about different calibrated datasets until the 10.2 m step. By the 30.6 m scale, the most extreme overestimations have been smoothed out, and the two parameters converge to similar distributions.

Turbulent fluxes show similar behaviours to those of the Upscaled Outputs, with smaller variation coefficients, mainly for the Latent Heat and higher resolutions. This may be attributed to the loss in spatial heterogeneity caused by the upscaling process: working on less heterogeneous input data, the model provides less heterogeneous outputs. By comparison, the more diverse aggregated outputs descend from already-diverse data modelled at high resolution.

These concepts are less visible for the Soil Moisture, as evident by its similarity. The difference is minimal because of the reduced soil moisture dynamics due to the brevity of the simulated period. Most pixels retain values very close to those of the starting condition, which is obviously uninfluenced by the upscaling approach.

Upscaled Outputs

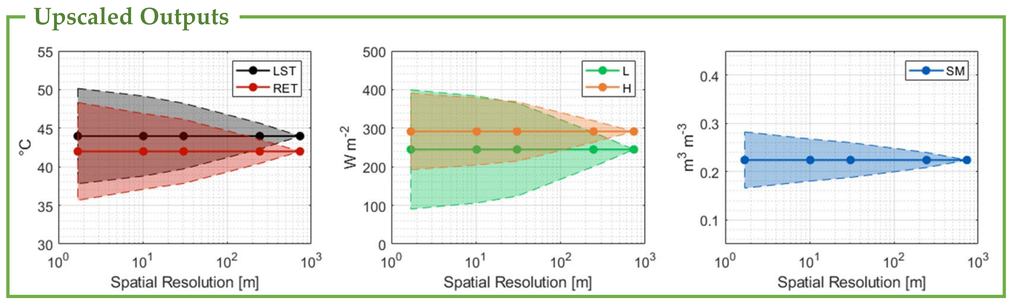

Upscaled Inputs

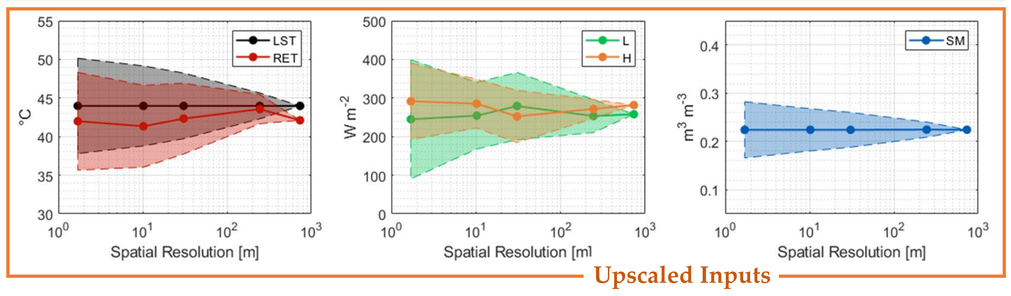

Scale	Min. Stomatal Res.		Soil Surface Res.		LST	RET (UI)	RET (UO)	L (UI)	L (UO)	H (UI)	H (UO)	SM (UI)	SM (UO)
1.7 m (Original)	127 s/m	59%	500 s/m	0%	14%	-	-	-	-	-	-	-	-
1.7 m (Calibrated)	579 s/m	63%	603 s/m	63%		15%	15%	63%	63%	34%	34%	26%	26%
10.2 m	410 s/m	51%	407 s/m	52%	12%	13%	12%	34%	57%	22%	30%	19%	20%
30.6 m	355 s/m	58%	355 s/m	58%	10%	11%	10%	31%	49%	27%	26%	16%	16%
244.8 m	399 s/m	25%	399 s/m	25%	4%	4%	4%	17%	18%	9%	10%	7%	7%
734.4 m	310 s/m	-	310 s/m	-	-	-	-	-	-	-	-	-	-

Average value and Variation Coefficient (VC) of the calibration parameters for the UI process across all scales.

Scale variability of the LST data and the UI and UO versions of four FEST-EWB outputs – Representative Equilibrium Temperature (RET), Latent Heat (L), Sensible Heat (H) and Soil Moisture (SM) – expressed in terms of Variation Coefficient (VC)

5b. Scale analysis

In the plot below, green dots identify the average temperature biases (model RET against flight LST) obtained by the Upscaled Outputs approach. The area highlights the one-standard-deviation-range around the mean value (±σ). As already discussed, the averaging process preserves the global mean. On the other hand, the orange dots provide the average temperature biases for the Upscaled Inputs approach, with the orange areas identifying the standard deviation range as above. The independent calibrations that produce the UI results, although completely unrelated to the UO data, provide quite similar temperature biases. For high resolutions (10.2 m and 30.6 m) the average biases are particularly close to the UO results. Coarser resolutions lose some of that similarity (in particular on 3rd September), but the overall comparison of the two datasets remains remarkable. Generally, low (absolute) biases can be attained with either of the upscaling approaches, as in both the error-minimization calibration rationale is employed.

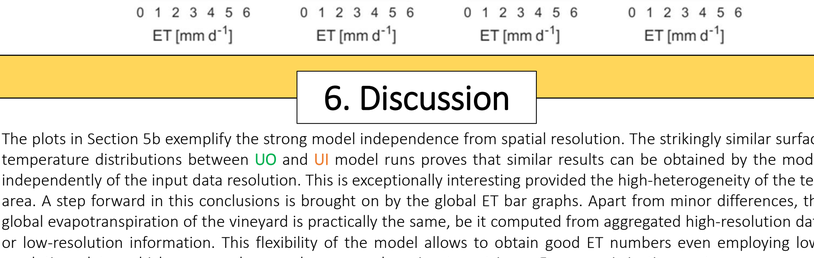

The comparison between the two approaches is investigated also in terms of daily evapotranspiration, focusing on the main vineyard area. The golden bar identifies the calibrated-model ET result for the native resolution (1.7m); the green bar identifies the Upscaled Outputs approach result, while the orange one the Upscaled Inputs result. The UO and UI results are never equal, but they are fundamentally never far from each other. Varying on the days, the differences can be more or less marked, but the overall value is similar, with no clear over-estimation of one over the other. Furthermore, both values are generally in the vicinity of the daily evapotranspiration computed at the highest resolution. The highest (10.2m) and lowest (734.4m) resolutions are the best-performing ones, but the global results do not seem to depend on the selected spatial resolution.

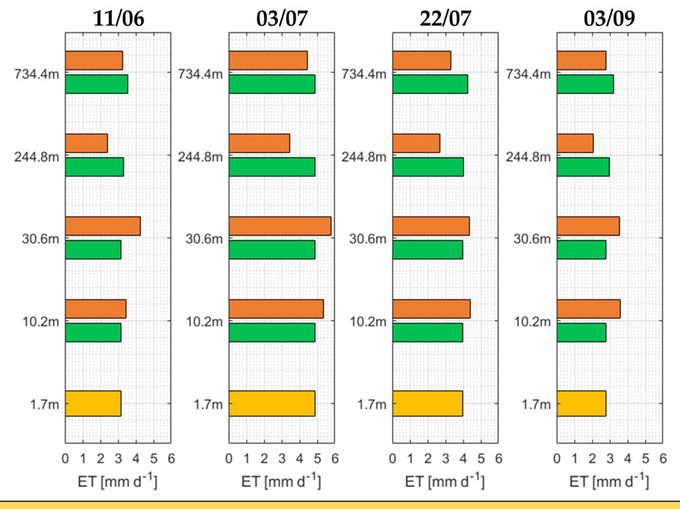

6. Discussion

The plots in Section 5b exemplify the strong model independence from spatial resolution. The strikingly similar surface temperature distributions between UO and UI model runs proves that similar results can be obtained by the model independently of the input data resolution. This is exceptionally interesting provided the high-heterogeneity of the test area. A step forward in this conclusions is brought on by the global ET bar graphs. Apart from minor differences, the global evapotranspiration of the vineyard is practically the same, be it computed from aggregated high-resolution data or low-resolution information. This flexibility of the model allows to obtain good ET numbers even employing low-resolution data, which commonly are cheaper and easier to retrieve. From an irrigation water management perspective, this means being able to enforce a continuous and accurate control over the crop with moderate costs.

Conclusions

(1) FEST-EWB has shown the ability of effectively interpreting land surface temperature even at coarse spatial resolutions and in highly-heterogeneous fields, thanks to its balances partition mechanism between vegetated and non-vegetated portions of each pixel. (2) Water irrigation management, if employing hydrological modelling, can be accurately performed with frequent, low-resolution satellite data, requiring a low effort and cost in data retrieval.

References

[1] G Ciraolo et al. (2012) – *Mapping ET on vineyards: a comparison between Penman-Monteith and Energy Balance approaches for operational purposes* – Rem. Sens. for Agr., Ecos. and Hydr., doi:10.1117/12.974967
[2] A Maltese, C Cammalleri, F Capodici, G Ciraolo, G La Loggia (2010) – *Surface soil humidity retrieval using remote sensing techniques: a triangle method validation* – Rem. Sens. for Agr., Ecos. and Hydr., doi:10.1117/12.865089
[3] C Corbari, G Ravazzani, M Mancini (2011) – *A distributed thermodynamic model for energy and mass balance computation: FEST-EWB* – Hydrological Processes, 25, 1443-1452 (2011), doi:10.1002/hyp.7910